Pergamon

Electrochimica Acta, Vol. 43, Nos 21–22, pp. 3193–3207, 1998

Printed in Great Britain
PII: S0013-4686(98)00007-3
0013-4686/98 $19.00 + 0.00

Studies of electrochemical properties of TiNi alloy used as an MH electrode — I. Discharge capacity

C. S. Wang*, Y. Q. Lei and Q. D. Wang

Department of Materials Science and Engineering, Zhejiang University, Hangzhou, 310027 P.R. China

(Received 29 October 1997; in revised form 12 January 1998)

Abstract—The electrochemical properties of TiNi alloy used as an MH electrode were investigated. A mathematical model for the electrochemical discharge capacity of TiNi electrode was developed. The model was used to study the effects of various parameters on the discharge capacity, and cycle life. The predicted results from the model fit well with the experimental results. Increasing the discharge current density and charge/discharge cycling current density decreases the discharge capacity, but a high charge/discharge cycling current density increases the cycle life of the hydride electrode. Increasing the exchange current density, or the diffusion coefficient of hydrogen or reducing the particle size increases the discharge capacity. Upon increasing the discharge current density the controlling steps of discharge capacity change from hydrogen diffusion in α phase (including oxide film) to the charge-transfer reaction on the hydride electrode surface. However for the TiNi alloy electrode the discharge capacity still depends mainly on the diffusion ability of hydrogen even at high discharge current density (200 mA/g). There exists an optimum dissolved hydrogen content of the α phase, $C_{\alpha\beta}^{opt}$, at which the discharge capacity reaches a maximum value. Also $C_{\alpha\beta}^{opt}$ increases with increasing discharge current density. © 1998 Elsevier Science Ltd. All rights reserved

LIST OF SYMBOLS

$C_{\alpha\beta}$, $C_{\beta\alpha}$	The hydrogen concentration of α or β phase equilibrating with P_{eq} at the interface between the α and β phase (mol cm^{-3})
$C_{\alpha\beta}^{opt}$	Optimum value of $C_{\alpha\beta}$, at which the discharge capacity getting the maxim (mol cm^{-3})
C_{max}	Hydrogen concentration of β phase equilibrating with 1 atm pressure (mol cm^{-3})
C_α	Actual hydrogen concentration of α phase at the interface between the α and β phase (mol cm^{-3})
C_s	Hydrogen concentration of α phase on the surface of particle (mol cm^{-3})
C_{OH}, C_{H_2O}	Concentration of OH^- and H_2O (mol cm^{-3})
D_α^A	Apparent hydrogen diffusion coefficient in α phase including hydrogen diffusion though the oxide film on the surface and transfer from the absorbed sites to adsorbed sites (cm^2 s^{-1})
Q_d, Q_{max}	Discharge capacity and the maxim discharge capacity, (mA h g^{-1})
Q_{abs}	Maximum capacity of hydrogen absorption for the hydride electrode.
F	Faraday's constant, 96547.6 (J V^{-1} mol^{-1}), or 26800 (mA h mol^{-1})
f	Ratio of $\frac{\partial Q_d}{\partial I_o}$ to $\frac{\partial Q_d}{\partial (D_\alpha^A/r_o^2)}$ (g mA^{-1} s^{-1})
I_d	Discharge current density (mA g^{-1})
I_c	Charge/discharge cycling current density (mA g^{-1})
I_o	Exchange current density (mA g^{-1})
$1/k$	Barrier coefficient of phase transformation (mol s g^{-1})
K_m	Percentage of active alloy.
m	Particle numbers
r_o	Average radius of the particle (cm).
r_α	Radius of unreacted β phase in discharge process (cm).
γ_c	Decline coefficient of maximum discharge capacity.
γ_k	Decline coefficient of kinetics.
ρ	Density of TiNi alloy (g cm^{-3}).
η	Overpotential V
w	weight per mole of the TiNi alloy (106.68 g mol^{-1}).

INTRODUCTION

Much attention has recently been given to nickel-hydride batteries using hydrogen storage alloys as the

*Author to whom correspondence should be addressed. Fax: +86 5717951358; E-mail: phycsw@ema.zju.edu.c.n

negative electrode materials due to the demand for portable power sources with high energy density, high-rate dischargeability, long cycle behavior, and better environmental compatibility. The titanium-based alloy TiNi has been known as one of the most promising hydrogen storage materials [1].

The electrochemical reactions taking place at the metal–electrolyte interface, the pressure–composition isotherms of electrode alloys, the diffusion of hydrogen and the phase transformation within the bulk of a hydrogen storage alloy are the main factors affecting the performances of a metal hydride electrode [2]. Yang *et al.* [3, 4] have established the relationship between the hydrogen surface concentration and overpotential for the galvanostatic discharge of non-porous hydride electrodes. Viitanen [5] developed a model for the discharge of a cylindrical metal-hydride electrode that took into account the ohmic losses in the electrolyte and in the solid materials, the charge-transfer reaction on the surface of the solid particles, and diffusion of atomic hydrogen in the solid particles. Considering the hydride electrode as a porous electrode, Vidts *et al.* [6], on the assumption that the charge-transfer reaction occurred on the surface of the metal-hydride particles, developed equations which included the mass transfer in the electrolyte and in the solid metal-hydride particles, the ohmic loss in the electrolyte and in the solid phase. However in all the studies mentioned above the effects of the activation and degradation were neglected altogether.

It is generally accepted that many factors affect the activation and degradation processes of MH electrodes. Considering the oxidation of hydrogen-absorbing metallic elements as the main cause for capacity deterioration of hydride electrodes, Willems [7], Wakao and Yonemura [8] and Züttel *et al.* [9] proposed their own cycle life equations. However, as the values of the parameters in these equations were determined only from experimental capacity data, they belong to semiempirical models. In our previous studies [2], we presented a mathematical model describing the relationship of discharge capacity to discharge current density and cycle number of a hydride electrode. But the effect of the charge/discharge cycling current density on cycle life was neglected.

Applying fundamental electrochemical principles to an oxide-covered metal electrode and phase transformations, a mathematical model for the discharge capacity of the TiNi electrode is presented here. The electrochemical parameters, including the exchange current density, the diffusion coefficient of hydrogen, the resistance of phase transformation, are all determined from the experimentally determined electrochemical properties of TiNi electrodes.

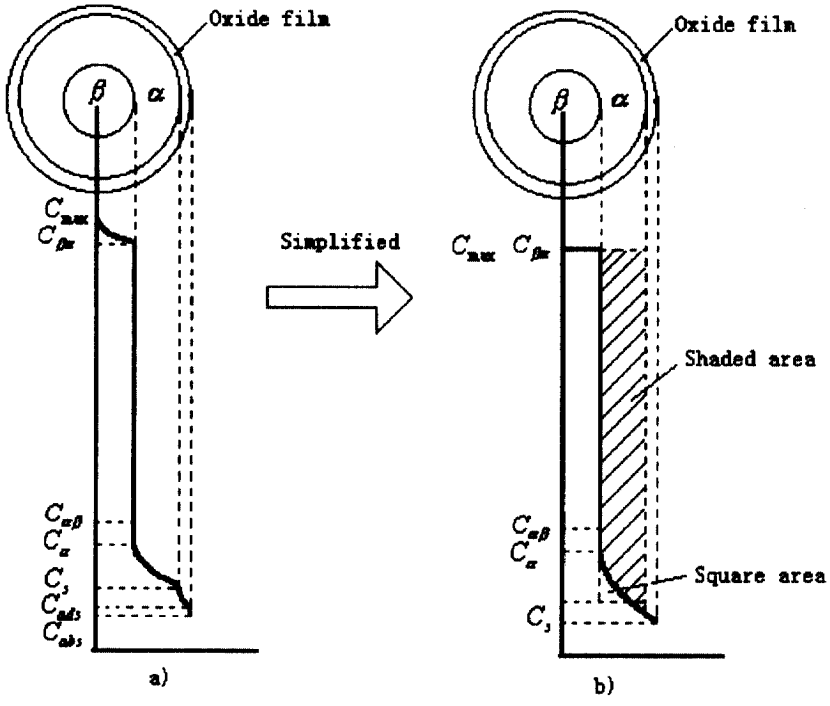

Fig. 1. Schematic diagram of hydrogen concentration in a spherical metal-hydride particle. (a) actual concentration of hydrogen distribution, (b) simplified concentration of hydrogen distribution.

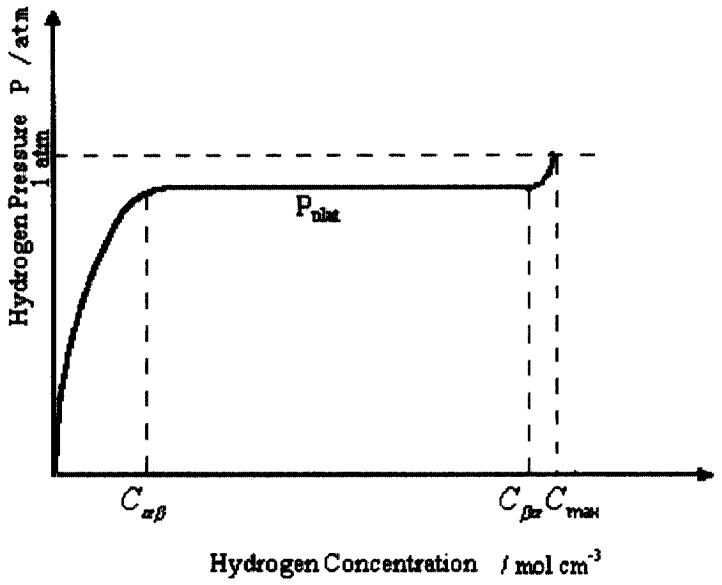

Fig. 2. Typical curve of pressure vs hydrogen content for metal-hydride electrode.

MODEL DEVELOPMENT

For thin porous electrodes, the mass transfer of OH^- and H_2O and the ohmic drop in the electrolyte have little effect on the electrode potential due to the large diffusion coefficients of OH^- and H_2O and the high porosity of the metal-hydride electrode [6]. The discharge process of a hydride electrode in this case can be simply treated as the discharge of hydrogen from MH particles.

Figure 1 shows a metal-hydride particle in the electrode modeled in this work and Fig. 2 shows the typical pressure–composition isotherm for the electrode alloy.

The hydrogen desorption process during discharge proceeds in the following sequence [2]:

(a) nucleation and growth of the α phase from β phase, the rate of which mainly depends on the difference of hydrogen concentration ($C_{\alpha\beta}$–C_α) and number of non-equilibrium defects, such as excess vacancies, dislocations, stacking faults and inclusions in the alloy, which for simplicity will not be discussed any further.

(b) diffusion of hydrogen from the α phase through the oxide film to the near-surface region of the particles [10, 11]. The drastic drop of hydrogen concentration in the TiO_2 film (Fig. 1(a)) is due to the much lower diffusivity of hydrogen in TiO_2 compared with that in the alloy [12].

(c) Transfer of hydrogen from the absorbed site in the near-surface region to adsorbed site on the electrode surface [3, 4];

$$MH_{abs} \Leftrightarrow MH_{ads}$$

For simplicity, the low hydrogen diffusivity in the oxide film and hydrogen transfer from the absorbed state to adsorbed state are treated together as the apparent diffusion coefficient of hydrogen in the α phase $D_\alpha{}^A$ (see Fig. 1).

(d) electrochemical oxidation of hydrogen at the electrode surface;

$$MH_{ads} + OH^- \Leftrightarrow M + H_2O + e$$

It is generally believed that part of the titanium in the TiNi alloy is segregated to the surface and exists in the form of oxide in 6 M KOH electrolyte after electrochemical cycling [13]. When the oxide film is thin, electrons are exchanged with the underlying metal itself, and the oxide film acts as a barrier for electron transfer, causing the exchange current density to decrease strongly as the film thickness grows [14].

Let us assume that the hydride particles are spherical, with an average radius r_o, and that the reaction occurs on the entire spherical surface uniformly, and the discharge process is in the quasi-steady state. The hydride electrode is cycled using the same charge and discharge current density I_c, but the discharge capacity is measured at discharge current density I_d. The discharge begins at the hydrogen concentration C_{max}, which is the hydrogen concentration in the alloy when it is fully charged uniformly throughout the entire β region with hydrogen pressure equaling 1 atm for open cells. When the pressure plateau of hydrogen is near to 1 atm, for approximation we can take C_{max} as $C_{\beta\alpha}$, which is the hydrogen concentration of the phase hydride equilibrated with the α phase at the plateau pressure P_{plat}, (see Fig. 2). For AB_5 type metal-hydride electrodes the above treatment is quite reasonable, but for the TiNi alloy electrode

some further approximations had to be made as no obvious pressure plateau is observed as shown in Fig. 3. For simplicity, we take the pressure at the median of hydrogen composition (H/M = 0.45) as the plateau pressure of the TiNi alloy electrode, and still let $C_{\beta\alpha}$ equal C_{max} and the first knee point of *P–C–T* curve be considered as $C_{\alpha\beta}$. For TiNi alloy the $C_{\alpha\beta}$ is measured to be H/M = 0.1 (see Fig. 3).

The distribution of hydrogen in the α-phase (including the oxide film)

From the continuity of H flow in the α-phase (including the oxide film) and Fick's first law [2];

$$4\pi r^2 m K_m D_\alpha^A \frac{dc}{dr} = 4\pi r_o^2 m K_m D_\alpha^A \frac{dc}{dr}\bigg|_{r=r_o} = \frac{4\pi r_o^3 \rho m K_m I_d}{3F} \quad (1)$$

where K_m is the percentage of active particles, F is Faraday's constant, mA h mol^{-1}, m is the number of spherical particles, ρ is density of TiNi alloy, g cm^{-3}, I_d is discharge current density, mA g^{-1}.

Integrating equation (1) with boundary condition $r = r_o$, $C = C_s$, $r = r_\alpha$, $C = C_\alpha$,

$$C_s = C_\alpha - \frac{I_d r_o^2 \rho}{3 D_\alpha^A F}\left(\frac{r_o}{r_\alpha} - 1\right) \quad (2)$$

where C_s is the hydrogen concentration (mol cm^{-3}) in the α phase on the electrode surface, C_α is the actual hydrogen concentration (mol cm^{-3}) in the α phase at the interface between the α phase and β phase mol/cm^3, r_α is the size of unreacted hydride.

When the electrode is discharged to the cut-off potential (–0.6 v), the surface concentration of hydrogen is close to zero, and the discharge capacity is equal to the value of F multiplied by the amount of hydrogen in the volume generated by the shaded area (Fig. 1). Also the shaded area can be approximated to the square area as indicated in Fig. 1. The discharge capacity Q_d is given by;

$$\begin{aligned} Q_d &\approx \frac{FK_m}{\rho}\left(C_{\beta z} - \frac{C_z}{2}\right)\left[1 - \left(\frac{r_z}{r_o}\right)^3\right] \\ &= \left(Q_{abs} - \frac{FK_m C_z}{2\rho}\right)\left[1 - \left(\frac{r_z}{r_o}\right)^3\right] \\ &= Q_{max}\left[1 - \left(\frac{r_z}{r_o}\right)^3\right] \end{aligned}$$

where Q_{abs} and Q_{max} are the maximum charge capacity and maximum discharge capacity of the hydride electrode respectively.

So the ratio of r_α to r_o is

$$\frac{r_\alpha}{r_o} \approx \left(1 - \frac{Q_d}{Q_{max}}\right)^{1/3} \quad (3)$$

Because hydrogen diffusion occurs radially in spherical particles and the interface between the α phase and β phase is incoherent, the growth rate of the α phase is [15]

$$r_\alpha \frac{dr_\alpha}{dt} = -\frac{k r_o^2}{\rho}(C_{\alpha\beta} - C_\alpha) \quad (4)$$

where $C_{\alpha\beta}$ is the hydrogen concentration (mol cm^{-3}) in the α phase equilibrated with hydride β at the plateau pressure P_{plat}, $1/k$ is the barrier coefficient of phase transformation.

In general, phase polarization is not very large, $C_\alpha \leq C_{\alpha\beta} \ll C_{\beta\alpha}$, hence

$$C_{\beta\alpha} - C_\alpha \approx C_{\beta\alpha} - C_{\alpha\beta} \quad (5)$$

From mass conservation at the boundary between the α and β phases

$$-(C_{\beta\alpha} - C_\alpha)\frac{dr_\alpha}{dt} = D_\alpha^A \frac{dc}{dr}\bigg|_{r=r_\alpha} = \frac{I_d r_o^3 \rho}{3 F r_\alpha^2} \quad (6)$$

Substituting equations (3)–(6) into equation (2), we obtain,

$$\begin{aligned} C_s = {} & C_{\alpha\beta} - \frac{I_d \rho^2 r_o}{3Fk r_\alpha (C_{\beta\alpha} - C_{\alpha\beta})} \\ & - \frac{I_d r_o^2 \rho}{3 D_\alpha^A F}\left[\left(1 - \frac{Q_d}{Q_{max}}\right)^{-1/3} - 1\right] \end{aligned} \quad (7)$$

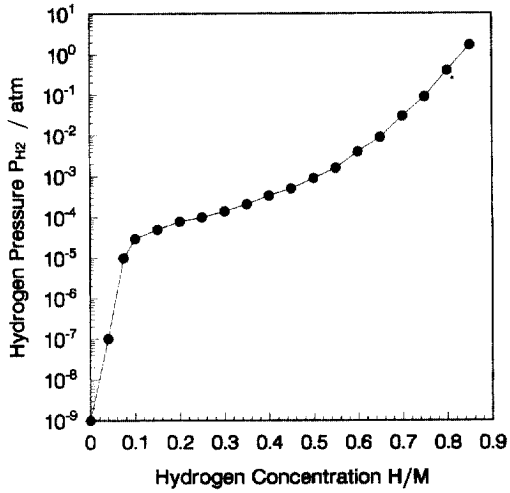

Fig. 3. Typical electrochemical discharge *P–C* curve at the 5th charge/discharge cycle and a cycle current density of $I_c = 50$ mA/g for TiNi hydride electrode.

Electrochemical reaction at the surface of the metal-hydride electrode

The current density due to the reaction is assumed to be given by a Bulter–Volmer expression [6]

$$I = I_o' \left\{ \frac{C_s C_{OH}}{C_{\alpha\beta} C^e_{OH^-}} \exp\left(\frac{\beta F}{RT}\eta\right) - \frac{C_{H_2O}}{C^e_{H_2O}} \exp\left[\frac{-(1-\beta)F}{RT}\eta\right]\right\} \quad (8)$$

where β is the symmetry coefficient, η is the overpotential, R is the gas constant, T is the absolute temperature, C_{OH^-} and C_{H_2O} are the concentrations of OH^- and H_2O in the solution, and $C^e_{OH^-}$ and $C^e_{H_2O}$ are concentrations of OH^- and H_2O at reference conditions.

As the change of C_{OH^-} in the anodic process is rather small and when the $\eta \gg RT/F$, equation (8) can be simplified to

$$I_d = I_o \frac{C_s}{C_{\alpha\beta}} \exp\left(\frac{\beta F}{RT}\eta\right) \quad (9)$$

Discharge capacity

Combining equations (7) and (9), Q_d can be written as

$$Q_d = Q_{max}\left[1 - \left(\frac{D^A_\alpha \rho}{k r_o^2 (C_{\beta\alpha} - C_{\alpha\beta})} + 1 \frac{3FD^A_\alpha C_{\alpha\beta}}{I_d \rho r_o^2}\left[1 - \frac{I_d}{I_o}\exp\left(-\frac{\beta F}{RT}\eta\right)\right] + 1\right)^3\right] \quad (10)$$

where

$$Q_{max} = \frac{FK_m}{\rho}\left(C_{\beta\alpha} - \frac{C_{\alpha\beta}}{2}\right)$$

EXPERIMENTAL PROCEDURES

The alloy was prepared by melting the Ti(purity 99.8%) and Ni(purity 99.9%) pellets in an arc furnace and remelting four times to assure homogeneity. The alloy pellets were pulverized first by electrochemical charging at low current density (10 mA g^{-1}) for 30 h and then mechanically milling. The alloy powder was sieved through 300 mesh. Metal hydride electrodes were made by mixing 100 mg alloy powder (< 300 mesh) with Cu powder (< 300 mesh) at a weight ratio 1:2 and cold pressing into pellets (d = 10 mm). For electrochemical measurements each pellet was attached to a copper rod of 5 mm diameter by a shrink sleeve and was positioned in a three-compartment glass open cell using Hg/HgO as the reference electrode. To reduce the ohmic potential drop between the working electrode and the reference electrode, a Luggin capillary was placed close to the hydride electrode in the working electrode compartment. A sintered nickel counter electrode was placed in a neighboring compartment separated by porous glass filter. The electrodes were charged and discharged electrochemically in 6 M KOH solution with temperature controlled at 25°C. The discharge capacity of the electrode was determined by the galvanostatic method.

Conventionally electrochemical pressure–composition curves were obtained by converting equilibrium potential to pressure on the basis of the Nernst equation from experimentally determined electrochemical data [16]. The equilibrium discharge potential curves were obtained by alternately performing the following two operations: (1) a pulse discharge of 25 mA/g × 0.25 h and (2) a rest period long enough for the potential to become constant. Discharge began at the potential corresponding to 1 atm hydrogen pressure and stopped when the potential dropped to –0.6 V with respect to Hg/HgO. A rest time of 0.5 h between charge and discharge was adopted [17].

The linear polarization experiments [18] were performed only on the 50% discharged state. After the open circuit potential was stabilized, I_o was determined at 25°C using the following equation under potentiodynamical conditions at scan rate of 1 mV s^{-1} with the overpotential within 10 mV.

$$I_o = \frac{I_d RT}{F\eta}$$

Determination of the D^A_α/r_o^2 ratio was performed with the pure α-phase. At first, the electrode was charged at 5 mA/g to the maximum hydrogen concentration of the α-solid solution (H/M ~ 0.1), 25 mA h/g) determined by P–C curves in several charge–discharge cycles. After a rest of half an hour, the electrode was discharged at a current density of 50 mA/g and the cut-off potential was –0.6 V vs Hg/HgO. D_α/r_o^2 is calculated from the charge left in the electrode by the following Equation [19];

$$Q_L = Q_o - Q_d = \frac{I_d r_o^2}{15 D^A_\alpha}$$

where Q_L is the charge (mA h g^{-1}) left in electrode mA h/g, Q_o is the initial capacity (mA h g^{-1}) and Q_d is the capacity discharged.

After certain charge–discharge cycles, the same measurements as above were conducted for the determination of I_o and $D_\alpha{}^A/r_o^2$ experiments.

DETERMINATION OF PARAMETERS

During activation cycles the surface area of alloy is increased by pulverization [20] and some of the

alloy components or their oxides are dissolved [9], which facilitates further activation together with the decrease in the activation energy barrier for phase transformation [2]. So I_o, D_α^A/r_o^2 and k all increase with charge–discharge cycling during the activation process.

The charge/discharge cycling also results in degradation, which is believed to be due to the loss of active alloy by oxidation, and the formation of an oxide film on the electrode surface that increases the contact electrical resistance. These factors cause I_o, D_α^A/r_o^2 and Q_{max} to decrease during charge–discharge cycling.

Concentration of hydrogen $C_{\alpha\beta}$, $C_{\beta\alpha}$ (mol/cm^3) and percentage of active material K_m

The relationship between $C_{\alpha\beta}$, $C_{\beta\alpha}$ and cycle number can be determined by the electrochemical P–C isotherms at different cycle numbers and K_m is determined by comparing the maximum concentration of hydrogen corresponding to 1 atm in electrochemical P–C–T curves with the maximum concentration of gaseous hydrogen at 1 atm pressure in gaseous P–C–T curves. Figure 3 shows the typical electrochemical discharge P–C curve at the 5th charge/discharge cycle and cycling current density $I_c = 50$ mA/g.

Comparing the electrochemical P–C curve in Fig. 3 with P–C–T curves at 20°C calculated from the thermodynamic data given by Burch [21], we estimate $K_m = 1$ [17] due to the high ratio of mixing Cu.

The maximum discharge capacity decreases with cycle number due to the oxidation of alloy. Supposing the maximum discharge capacity before oxidation of alloy is Q_{max0}, $\ln(Q_{max0}/Q_{max})$ is assumed to be proportional to the total charge–discharge time [21] which is equal to the single cycle time Δt multiplied by the cycle number N. Because the thickness of TiO_2 usually increases parabolically (square root function) with discharge time, it is reasonable to assume $\ln(Q_{max0}/Q_{max})$ increases parabolically with charge–discharge cycle time $(N \times \Delta t)$. Also Δt is inversely proportional to the charge/discharge cycling current density I_c.

$$Q_{max} = \frac{FK_m}{\rho}\left(C_{\beta\alpha o} - \frac{C_{\alpha\beta o}}{2}\right)\exp\left(-\frac{\lambda_Q N^{1/2}}{I_c^{1/2}}\right) \quad (11)$$

here I_c is the charge/discharge cycling current density (mA g^{-1}), Comparing equation (11) with Q_{max} in equation (10)

$$C_{\beta\alpha} = C_{\beta\alpha o}\exp\left(-\frac{\lambda_Q N^{1/2}}{I_c^{1/2}}\right)$$

$$C_{\alpha\beta} = C_{\alpha\beta o}\exp\left(-\frac{\lambda_Q N^{1/2}}{I_c^{1/2}}\right)$$

Figure 4 shows the experiment data of $C_{\alpha\beta}w/\rho$ and $C_{\beta\alpha}w/\rho$ at various cycling current densities

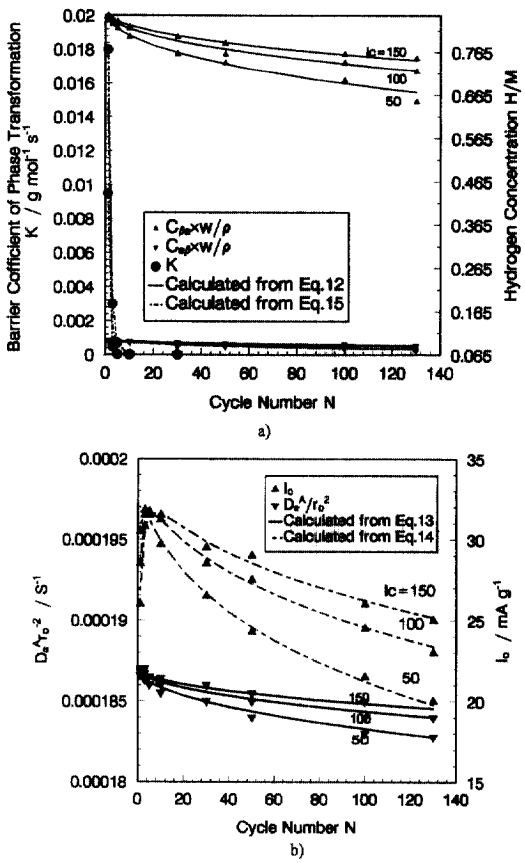

Fig. 4. Relationship between I_o, D_α^A/r_o^2, $C_{\alpha\beta}w/\rho$ and $C_{\beta\alpha}w/\rho$, k and cycle number at different current densities. (a) k, $C_{\alpha\beta}w/\rho$ and $C_{\beta\alpha}w/\rho$, (b) I_o and D_α^A/r_o^2.

determined by electrochemical P–C–T curves (black triangle), which have a good fit with equation (12) (solid line) with $\lambda_Q = 0.153$ and $C_{\beta\alpha o}w/\rho = 0.86$ H/M, $C_{\alpha\beta o}w/\rho = 0.1$ H/M, where ρ is the density of TiNi alloy (g cm^{-3}), and w is the weight per mole of TiNi alloy, (106.6 g mol^{-1}). Since $Q_{abs} = (FK_m/\rho)C_{\beta\alpha}$, therefor the calculated maximum capacity of hydrogen absorption also fit well with experimental data.

Factor of the apparent diffusion coefficient of hydrogen in α phase/the square of particle radius D_α^A/r_o^2 (s^{-1})

D_α^A/r_o^2 can be measured either by galvanostatic discharge or potentiostatic methods [18]. For galvanostatic model, the discharge capacity of TiNi electrode can be expressed as

$$Q_d = 25\exp\left(-\frac{0.153N^{1/2}}{I_c^{1/2}}\right) - \frac{r_o^2}{15D_\alpha^A}i_d$$

The above equation can only be used for a single phase substance (α or β phase) or after a very long discharge time when the β phase has been completely transformed to α phase. In our experiments the galvanostatic method was applied to a single α

Table 1.
The variation of Q_d with cycle number at $I_c = 50$ mA/g($= I_d$)

N	1	3	5	10	30	100	130
Q_d (mA h/g)	19.9	20	20.03	20.02	19.99	19.94	19.93

phase. The value of Q_d is shown in Table 1 at the cycle current density $I_c(=I_d) = 50$ mA.

The ratio D_α^A/r_o^2 after 1, 3, 5, 10, 30, 100, and 130 cycles with $I_c = 50$, 100, and 150 mA/g is shown in Fig. 4(b). In Fig. 4(b) a small increase of D_α^A/r_o^2 with cycle number during the activation process means that the pulverization of TiNi is low, which is in agreement with the results of our previous investigation [2]. After activation, D_α^A/r_o^2 decreases with cycle number due to an increase in the oxidation layer on the TiNi alloy electrode surface. The relationship of D_α^A/r_o^2 with I_c and N can be described simply by the following equation:

$$\frac{D_\alpha^A}{r_o^2} = 1.87 \times 10^{-4} \exp\left(-\frac{0.01414}{I_c^{1/2}} N^{1/2}\right) \quad (13)$$

Exchange current density I_o (mA/g)

For an oxide-covered metal-hydride electrode the exchange current density decreases, approximately exponentially, with increasing oxide film thickness [13]. For exchange current density, in all charge–discharge cycles, a linear dependence of overpotential on the discharge current density is found according to the simplified Butler–Volmer equation at small overpotentials. A typical example is given in Fig. 5. I_o can be calculated from the slope of the I vs η curves. The I_o values obtained at different cycle numbers and $I_c = 50$, 100, and 150 mA/g are also shown in Fig. 4(b). From Fig. 4(b) I_o values increase during activation and then decrease with cycle number. This agrees with the results for the $LaNi_{4.4}Cu$ electrode reported by Notten [22]. The relationship between the exchange current density and the cycling numbers can be expressed by the following equation.

$$I_o = 35 \times \left[\exp\left(-\frac{0.3535}{I_c^{1/2}} N^{1/2}\right) - 0.9 \times \exp\left(-\frac{17.7 N^{1/2}}{I_c^{1/2}}\right)\right] \quad (14)$$

The main reason for the increase in I_o is the increase of surface area [22] due to the pulverization during activation. Figure 5 shows the typical potentiodynamic (1 mV s^{-1}) current density–overpotential curve measured on a TiNi electrode at 50% discharge state, $I_c = 50$ mA/g, $N = 10$.

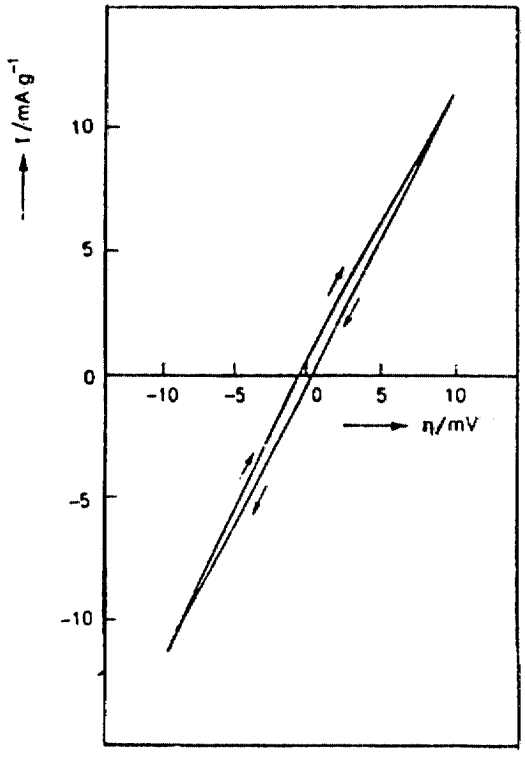

Fig. 5. Typical potentiodynamic (1 mV s^{-1}) current density–overpotential curve measured on a TiNi electrode at 50% state of discharge (SOD), $I_c = 50$ mAg^{-1}, $N = 10$, the arrows indicate the scan direction.

Barrier coefficient of phase transformation k^{-1} (mol g s^{-1})

The fact that the value of k increases with the charge–discharge cycle number during the activation process is probably due to the development of two-dimensional defects in the alloy. On the basis of the initial discharge capacity and of that after cycling, the value of k in equation (10) is determined using the following equation (see Fig. 4(a))

$$k = 4.16 \times 10^{-2} \exp\left(\frac{10.25N}{I_c^{1/2}}\right) \quad (15)$$

Kinetic equation of the TiNi electrode

Table 2 gives the values of the parameters. Substitute the above parameters into equation (10). The discharge capacity Q_d is

$$Q_d = 204(1 - \gamma_c)(1 - \gamma_k) \quad (16)$$

where $\gamma_c = 1 - \exp(-0.153 I_c^{-1/2} N^{1/2})$ is the decline coefficient of maximum discharge capacity caused by the decrease of $C_{\beta\alpha}$ and $C_{\alpha\beta}$ values due to oxi-

Table 2.
The values of parameters

Methods	Parameters	Unit	Value
$C_{\alpha\beta}w/\rho$	H/M	$0.1\exp(-0.153\,N^{1/2}I_c^{-1/2})$	*P–C–T* curves
$C_{\beta\alpha}w/\rho$	H/M	$0.86\exp(-0.153\,N^{1/2}I_c^{-1/2})$	*P–C–T* curves
Q_{max}	mA h g^{-1}	$204\exp(-0.153\,N^{1/2}I_c^{-1/2})$	*P–C–T* curves
	mA g^{-1}	$35[\exp(-0.3535\,N^{1/2}I_c^{1/2})$	line polarization
I_o		$-0.9\exp(-17.7\,N^{1/2}I_c^{-1/2})$	
D_α/r_o^2	s^{-1}	$1.87\times10^{-4}\exp(-0.01414\,N^{1/2}I_c^{-1/2})$	galvanostatic discharge
k	s mol^{-1} g^{-1}	$4.16\times10^{-2}\exp(10.25\,NI_c^{-1/2})$	discharge capacity
η	V	0.3	
RT	kJ mol^{-1}	2.474	
β		0.5	
K_m		1	
w	g mol^{-1}	106.6	
F	mA h mol^{-1}	26800	
	kJ V^{-1} mol^{-1}	96.5476	

dation of active metals, and where the decline coefficient of kinetics due to the decrease of $D_\alpha{}^A$ and I_o by oxidation can be expressed by the following equation.

$$\gamma_k=\left[\frac{0.63\times\exp(-0.13886I_c^{-1/2}N^{1/2}-10.25I_c^{-1/2}N)+1}{50.7\times\exp(-0.16714I_c^{-1/2}N^{1/2})[1/I_d-8.2\times10^{-5}/(\exp(-0.3535I_c^{-1/2}N^{1/2})-0.9\times\exp(-17.7I_c^{-1/2}N^{1/2}))]+1}\right]^3$$

One point is worth mentioning again, in the above equation: I_c is the charge/discharge cycling current density, and I_d is the discharge current density when the discharge capacity is measured. So I_c can change independently of I_d.

RESULTS AND DISCUSSION

Discharge capacity of the TiNi alloy electrode during a charge/discharge cycle

For measuring the cycling behavior of hydride electrodes, two methods are usually used: (a) the discharge capacity during charge/discharge cycling is tested at a high cycling current density, i.e. $I_c(=I_d)$ is high. (b) the hydride electrode is cycled at a high current density (I_c) but the discharge capacity after a certain number of cycles is tested at low discharge current density I_d. The effect of cycling current density I_c and discharge current density I_d on cycle behavior is discussed in this section.

Effects of cycling current density I_c on cycle behavior at $I_d=I_c$ and at $I_d=50$ mA/g

The relationship between discharge capacity of the TiNi alloy electrode, the cycling current density and the cycle number at $I_d=I_c$ is shown in Fig. 6. During activation the discharge capacity increases gradually and reaches its maximum between the 2nd and 5th cycle, depending on the cycling current density, and then decreases on further cycling, but the decline of discharge capacity becomes smaller when the cycling current density is high. The experiment values tested at $I_c(=I_d)=50$, 100, and 150 mA/g fit very well with calculated data from equation (16) as shown in Fig. 6(b).

We believe that the increase of discharge capacity during the activation process is caused by the decrease in the concentration polarization, which in turn is caused by phase transformation, and that the capacity decline after the alloy is fully activated is mainly caused by the corrosion of the TiNi alloy and the formation of an oxide film on the TiNi electrode surface, which jointly lower $C_{\beta\alpha}$, $C_{\alpha\beta}$, $D_\alpha{}^A$ and I_o. From equations (5)–(7) and Fig. 7, we can see that at certain cycling current I_c, the decreases of $C_{\beta\alpha}$ and $C_{\alpha\beta}$ are faster than $D_\alpha{}^A$ and I_o in charge/discharge cycling, and the γ_c/γ_k ratio increases as the number of cycles increases. But for a fixed cycle number, γ_c/γ_k decreases as the cycling current density increases, which means that at low cycling current the cycle life of the TiNi alloy electrode is mainly controlled by the decline in the maximum discharge capacity. However when the cycling current density is high the decline of discharge kinetics becomes the limiting factor for cycle life.

For cases other than $I_c=I_d$, results are quite different. At a fix discharge current density ($I_d=$)50 mA/g, both the cycle life and the discharge capacity increase with cycling current density as shown in Fig. 8. This is due to the lower oxidation rate at high cycling current density. Oxidation

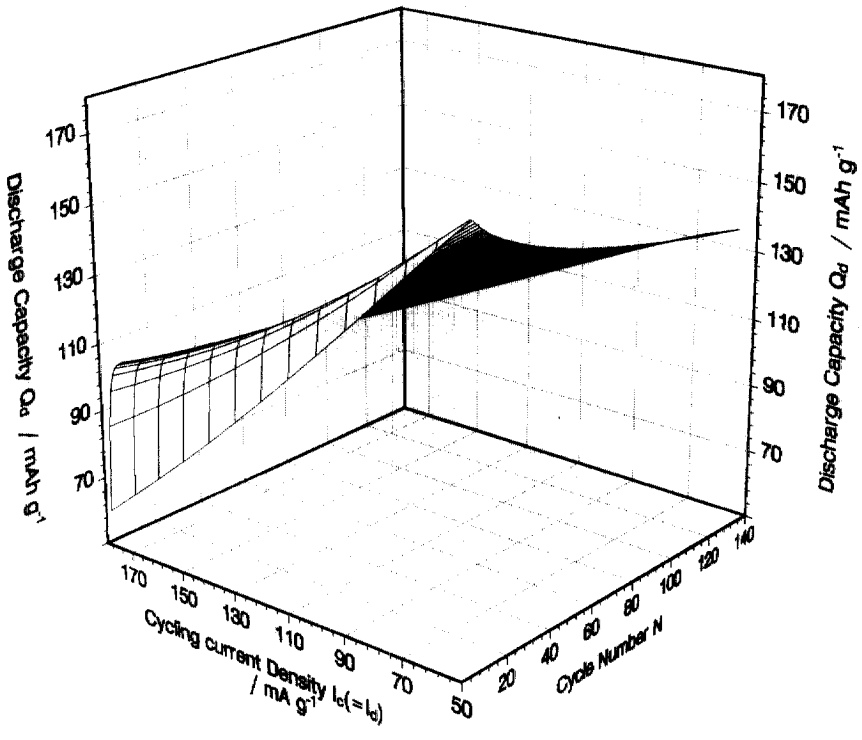

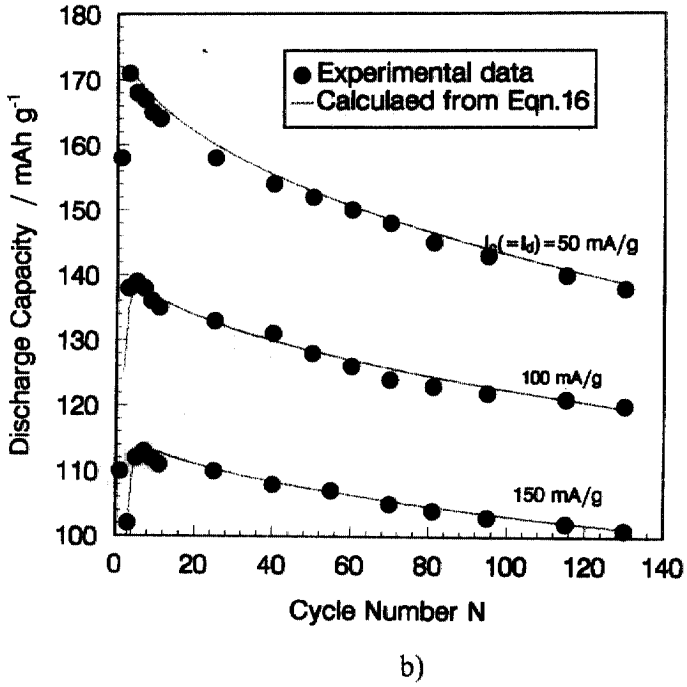

Fig. 6. Plot of the measured cycle life of the TiNi sample. (a) three-dimensional curved surface calculated from the model, (b) cycle life at cycling current density $I_c(=I_d)$ = 50, 100, and 150 mA/g, the black points in (b) express experimental data and the solid line is the theoretical curve calculated from equation (16).

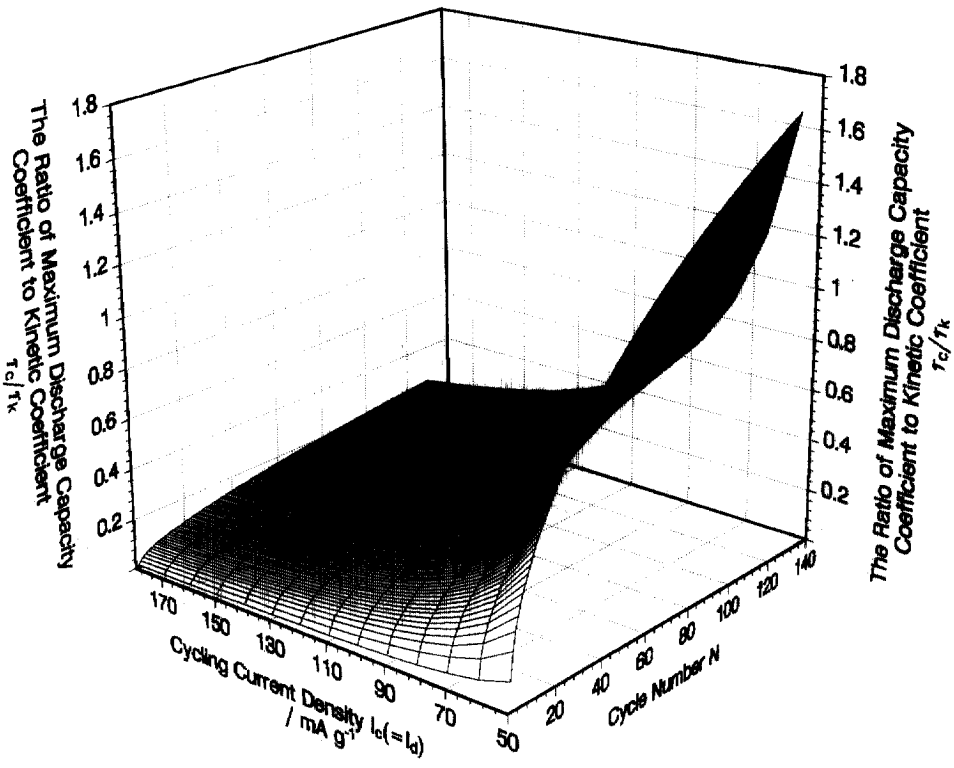

Fig. 7. The ratio of the coefficient of maximum discharge capacity to the coefficient of discharge kinetics (T_c/T_k) vs cycle number and cycling current density $I_c(=I_d)$.

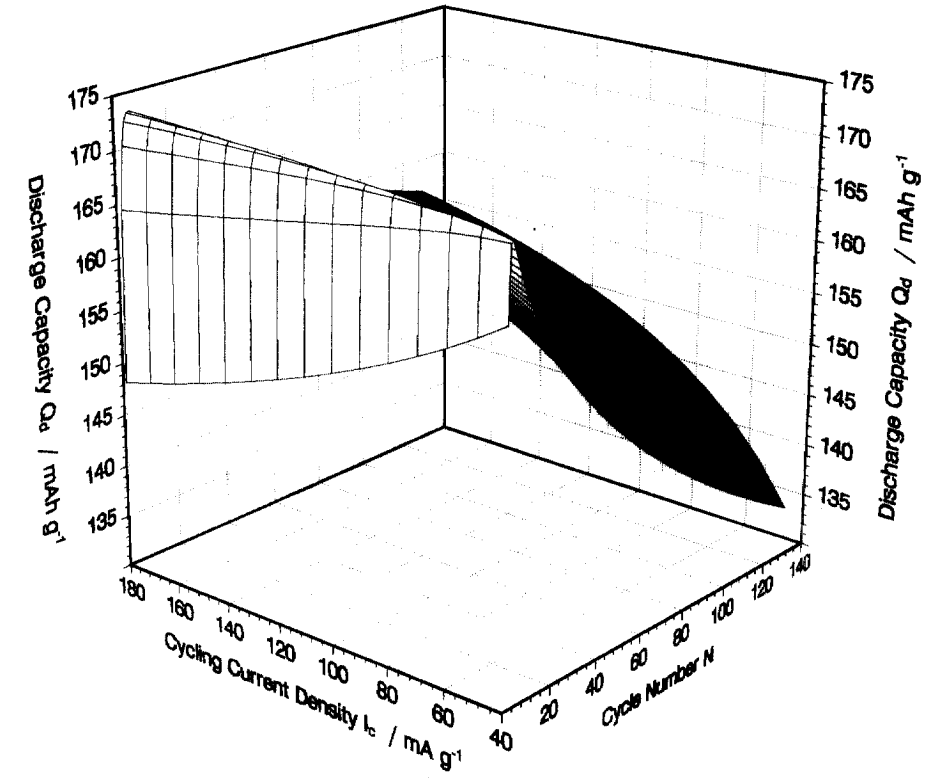

Fig. 8. Effects of the cycling current density I_c on cycle life at $I_d = 50\ \mathrm{mAg^{-1}}$.

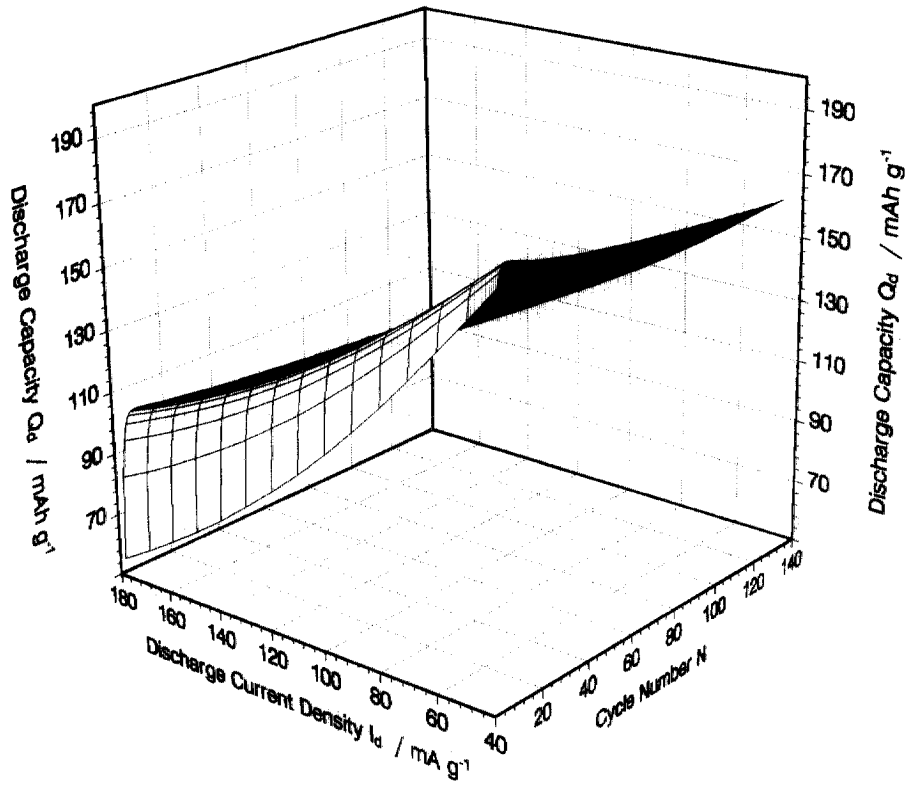

Fig. 9. Relationship between cycle life and discharge current density at cycling current density $I_c = 200$ mA g^{-1}.

during the discharge process at 50 mA/g is not considered in the curve of Fig. 8. So the actual cycle behavior is lower than the calculated data in Fig. 8.

The effects of discharge current density I_d on cycle behavior at $I_c = 200$ mA g^{-1}

The relationship between cycle behavior and discharge current density at cycling current density $I_c = 200$ mA g^{-1} is shown in Fig. 9, from which we find that the discharge capacity decreases with increase of discharge current density, but its cycle life is independent of the discharge current density, which is also caused by the effect of neglecting oxidation during discharge at current density I_d by equation (16). This is valid only when the cycle numbers are much larger than the number at which discharge capacity is measured.

DISCHARGE CAPACITY OF THE TiNi ELECTRODE AT $I_C = 50$ MA/G, $N = 10$

Effects of exchange current density and hydrogen diffusion coefficient on the discharge capacity at $I_c = 50$ mA/g, $N = 10$

Figure 10 shows the relationship between discharge capacity Q_d, I_o and D_α^A/r_o^2 at $I_c = 50$ mA/g, $N = 10$. In Fig. 10 we can see that increasing the particle size and reducing the value of the atomic hydrogen diffusion coefficient both affect the discharge capacity behavior in the same way, and the discharge capacity Q_d decreases with decreasing D_α^A/r_o^2 and I_o. At low discharge current density $I_d = 50$ mA/g, Q_d drops drastically with decreasing D_α^A/r_o^2 and I_o at about $D_\alpha^A/r_o^2 = 1.87 \times 10^{-4}$ (s^{-1}), $I_o = 2$ mA/g (see Fig. 10(a)), and the knee of I_o increases with discharge current density I_d and D_α^A/r_o^2. However when the discharge current density is high, the decreases of discharge capacity with reduction of D_α^A/r_o^2 become smoother gradually and finally the knee of D_α^A/r_o^2 disappears at a discharge current density 500 mA/g as shown in Fig. 10(c)). For the TiNi electrode with $I_o = 29.9$ mA/g, $D_\alpha^A/r_o^2 = 1.87 \times 10^{-4}$ (s^{-1}) at low discharge current density $I_d = 50$ mA/g, the discharge capacity mainly depends on D_α^A/r_o^2, (see Fig. 10(a)) but at high discharge current density, both I_o and D_α^A/r_o^2 control the discharge capacity (see Fig. 10(c)). Also the factor of $(\partial Q_d/\partial I_o)/(\partial Q_d/\partial(D_\alpha^A/r_o^2))$ can be calculated from equation (10).

$$f = \frac{\partial Q_d}{\partial I_o} \Big/ \frac{\partial Q_d}{\partial (D_\alpha^A/r_o^2)} = \frac{D_\alpha^A}{r_o^2 I_o}\left(\frac{I_d}{I_o \exp(\beta F/RT\eta) - I_d}\right) = \frac{D_\alpha^A}{r_o^2 I_o}\left(\frac{1}{I_{Le}/I_d - 1}\right) \quad (17)$$

where $\eta = 0.332$ V, I_{Le} is the electrochemical limit current density (mA g^{-1}).

The value of f reflects the relative effects of the charge-transfer reaction and hydrogen diffusion on discharge capacity. Larger values of f mean the

charge-transfer reaction is the factor controlling discharge capacity, and smaller f values indicate the discharge capacity is limited by hydrogen diffusion. In equation (17) the controlling influence changes from the hydrogen diffusion to the charge-transfer reaction with increasing discharge current density I_d. Also equation (17) can not be used for qualitative analysis because f is not dimensionless. From the above analysis we believe that at low discharge current density, the diffusion of hydrogen is the limiting factor, but at high discharge current density both the charge-transfer reaction at the electrode surface and the diffusion of hydrogen control the discharge capacity. As the discharge current density increases further the charge-transfer reaction at the electrode surface may become the controlling factor in discharge capacity (more details are discussed in part II). This prediction is in agreement with the generally accepted result that enhancing the electrocatalytic performance of the hydride electrode would obviously increase the high-rate dischargeability [18, 23]. For the TiNi electrode with $I_o = 29.9$ mA g^{-1} at $I_c = 50$ mA g^{-1}, $N = 10$, the diffusion of hydrogen is still a controlling factor in discharge capacity even at a much higher discharge current density $I_d = 200$ mAg^{-1} (see Fig. 10(b)). Thus for the TiNi electrode the key problems are to maintain the electrocatalytic performance of the TiNi electrode alloy during charge/discharge cycling and to improve the diffusion ability of hydrogen. Although reducing the particle size r_o can increase D_α^A/r_o^2, it also increases the rate of oxidation of the TiNi alloy and reduces the stability of electrocatalytic properties of the TiNi alloy in charge/discharge cycles.

Effect of maximum hydrogen concentration of the α phase $C_{\alpha\beta}$ on discharge capacity at $I_c = 50$ mA/g, $N = 10$

For electrodes based on TiNi alloys the value of $C_{\alpha\beta}$ can be adjusted by partial substitution of other metals for Ti or Ni. From equation (10), we believe that the large $C_{\alpha\beta}$ decreases the maximum discharge capacity Q_{max}, but increases the discharge kinetics, so there may exist an optimum value of $C_{\alpha\beta}$, at which the discharge capacity reaches a maximum. Figure 11 show the relationship of discharge capacity with $C_{\alpha\beta}$ and discharge current density I_d. The discharge capacity increases initially with $C_{\alpha\beta}$ and then decreases. At a low discharge current density 50 mA/g the discharge capacity increases by about 4% (from 166.4 to 172 mA h/g) when $C_{\alpha\beta}$

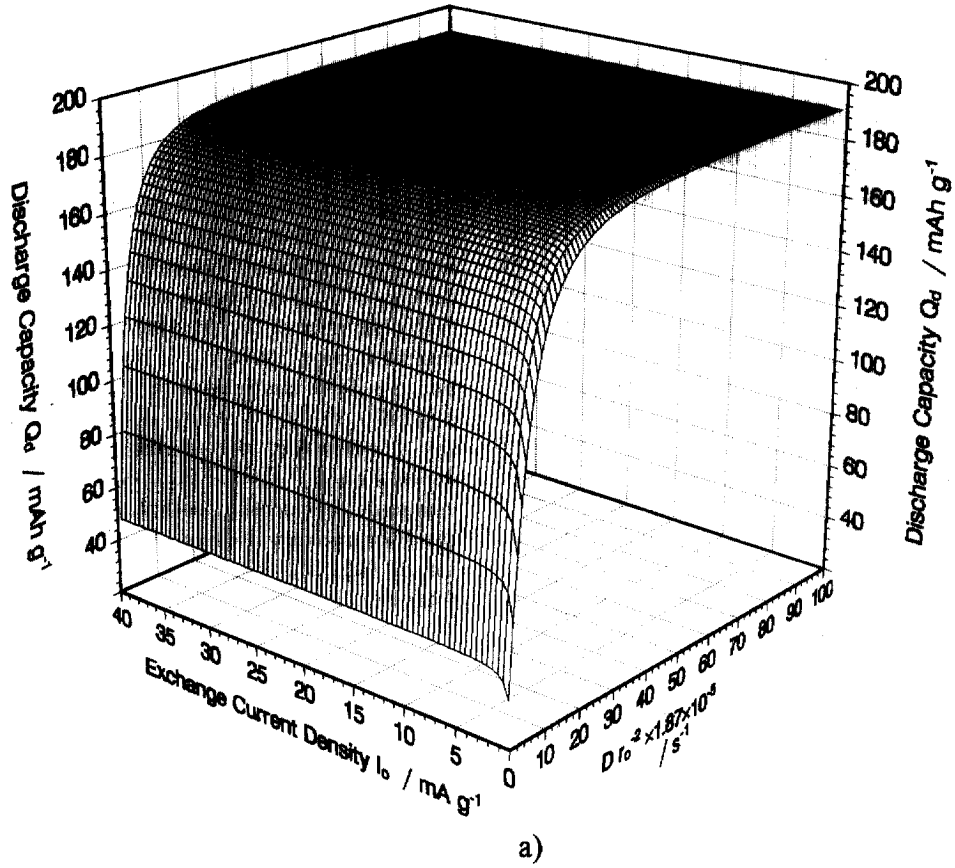

Fig. 10. Relationship between discharge capacity Q_d, I_o and D_α^A/r_o^2 at $I_c = 50$ mA g^{-1}, $N = 10$. (a) discharge current density $I_d = 50$ mA g^{-1}, (b) $I_d = 200$ mA g^{-1}, (c) $I_d = 500$ mA g^{-1}.

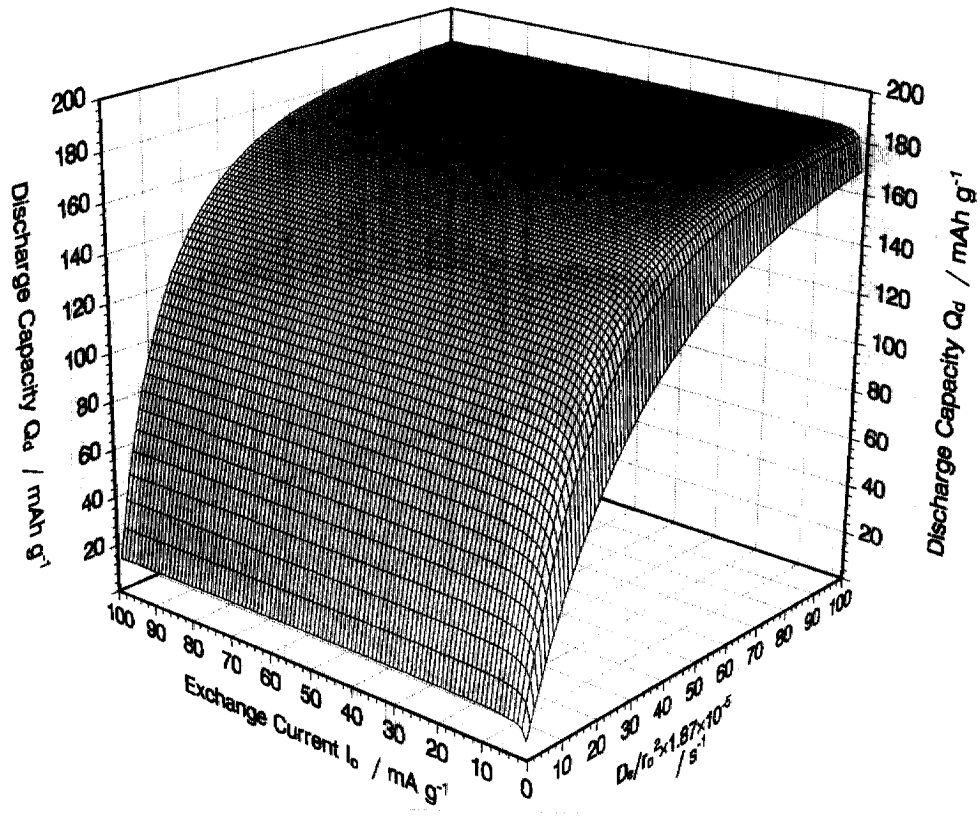
Discharge Capacity Q_d / mAh g^{-1}
200
180
160
140
120
100
80
60
40
20
100 90 80 70 60 50 40 30 20 10 0
Exchange Current I_o / mA g^{-1}
10 20 30 40 50 60 70 80 90 100
$D_H/l_o^2 \times 1.87 \times 10^{-5}$ / s^{-1}
Discharge Capacity Q_d / mAh g^{-1}

b)

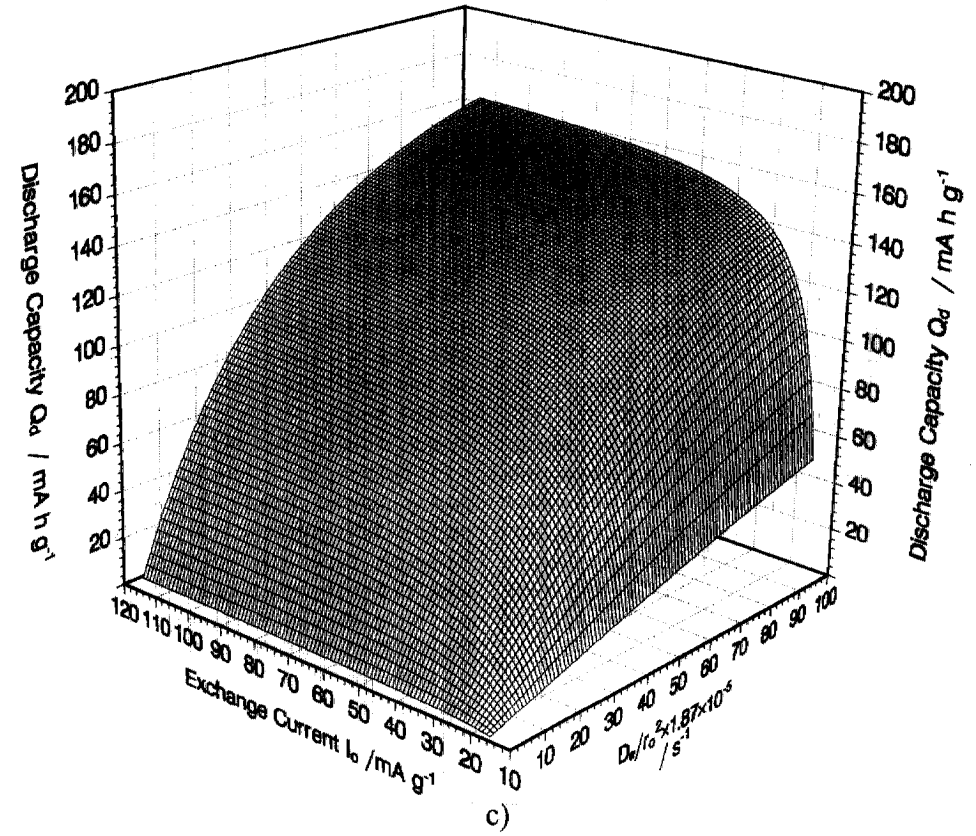
Discharge Capacity Q_d / mA h g^{-1}
200
180
160
140
120
100
80
60
40
20
120 110 100 90 80 70 60 50 40 30 20 10
Exchange Current I_o /mA g^{-1}
10 20 30 40 50 60 70 80 90 100
$D_H/l_o^2 \times 1.87 \times 10^{-5}$ / s^{-1}
Discharge Capacity Q_d / mA h g^{-1}

c)

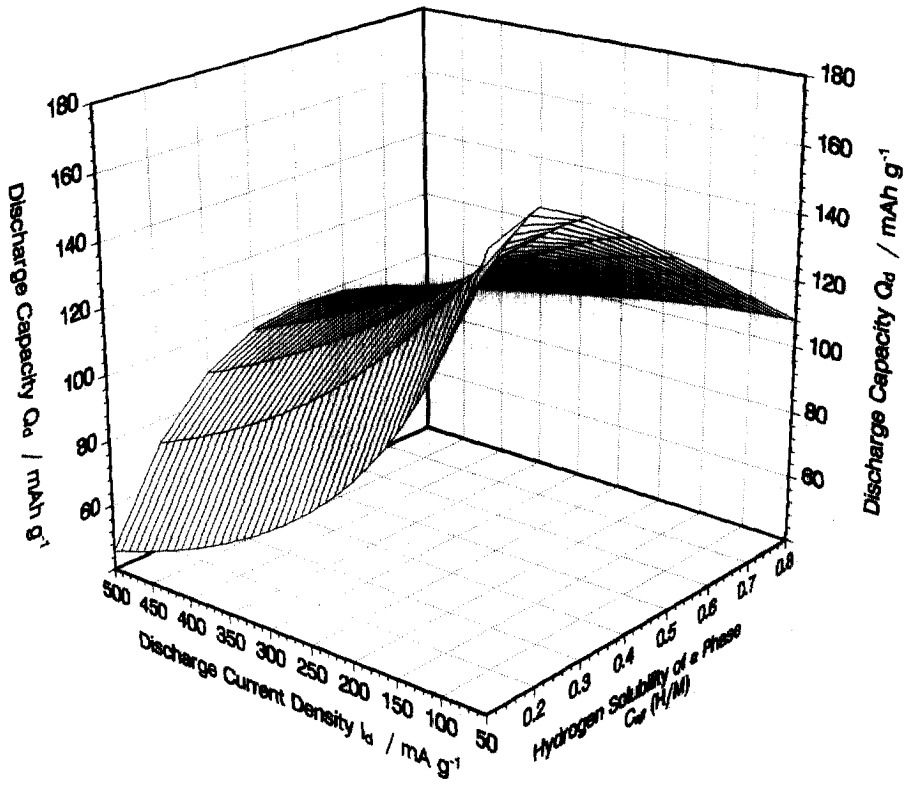

Fig. 11. Relationship between discharge capacity Q_d, $C_{\alpha\beta}$ and discharge current density I_d.

changes from H/M = 0.1 to 0.2, but at a high discharge current density 500 mA/g, the discharge capacity increases by 117% (from 45.7 to 99.2 mA h/g) as $C_{\alpha\beta}$ change from H/M = 0.1 to 0.5. So enhancement of hydrogen solubility in the α phase within H/M = 0.5 obviously improves the rate capacity. Also $C_{\alpha\beta}^{opt}$ (optimum value of $C_{\alpha\beta}$) increases from H/M = 0.2 to 0.5 with increasing discharge current density I_d from 50 to 500 mA/g. The predicted influences of $C_{\alpha\beta}$ on discharge capacity at different discharge current density have been proved by the experimental results on the TiV_3Ni_x ($x \leq 0.75$) electrode alloy as reported by Tsukahare [1]. From Fig. 4 in Ref. [1], $C_{\beta\alpha}$ decreases with the increase of the nickel content. This means the discharge capacity is decreased. But in fact the discharge capacity increases with nickel content first and then decreases, because $C_{\alpha\beta}$ also increases with nickel content. A larger $C_{\alpha\beta}$ enhances the high-rate dischargeability of the TiV_3Ni_x alloy (see Fig. 5 in Ref. [1]). This agrees well with the predicted results based on our model.

CONCLUSION

(1) equation (16), which is deduced from electrochemical and phase transformation principles fits well with the experimental data measured on TiNi alloy. The model can be used to analyze the effects of important factors in the discharge process of the TiNi alloy electrode.

(2) For the TiNi alloy electrode the operating discharge capacity is influenced by the maximum discharge capacity of the alloy and the discharge kinetics which is determined by the electrochemical polarization and concentration polarization; this in turn depends on both the diffusion ability of hydrogen and the rate of phase transformation. The activation is mainly controlled by phase transformation, and the cycle life at low cycling current density is mainly determined by the decline in the maximum discharge capacity, but when cycling current density are high, the cycle life is controlled by the decline in the discharge kinetics.

(3) Increase in the discharge current density and cycling current density decrease the discharge capacity, but improve the cycle life behavior. Although the charge-transfer reaction on the TiNi alloy electrode surface becomes a more limiting factor when the discharge current density increases, the discharge capacity is still mainly dependent on the diffusion of atomic hydrogen from the bulk to the surface of the particles even at 200 mA/g discharge current density. Therefor the electrocatalytic ability of the TiNi electrode is high enough even at high discharge current density, 200 mA g^{-1}. The key problems are how to maintain the electrocatalytic performance during charge/discharge cycling and

how to improve the diffusion ability of hydrogen in the α phase.

(4) From this model we infer that increasing the solubility of hydrogen in the α phase (oxide film included) within a certain range enhances the capacity at high discharge current density for the TiNi electrode. There exists an optimum soluble hydrogen content in the α phase $C_{\alpha\beta}^{opt}$, at which the discharge capacity reaches a maximum value. This also agrees well with experimental results reported by Tsukahara *et al.* [1].

ACKNOWLEDGEMENTS

The authors acknowledge the financial support from the National Natural Science Foundation of China.

REFERENCES

1. M. Tsukahara, K. Takahashi, T. Mishima, T. Sakai, H. Miyamura and N. Kuriyama, *J. Alloys Comp.* **226,** 203 (1995).
2. Y. Q. Lei, C. S. Wang, X. G. Yang, H. G. Pan, J. Wu and Q. D. Wang, *J. Alloys Comp.* **231,** 611 (1995).
3. Q. M. Yang, M. Ciureanu, D. H. Ryan and J. O. Stromolsen, *J. Electrochem. Soc.* **141,** 2111 (1994).
4. Q. M. Yang, M. Ciureanu, D. H. Ryan and J. O. Stromolsen, *J. Electrochem. Soc.* **141,** 2116 (1994).
5. M. Viitanen, *J. Electrochem. Soc.* **140,** 936 (1993).
6. P. D. Vidts, J. Delgado and R. E. White, *J. Electrochem. Soc.* **142,** 4006 (1995).
7. J. J. G. Willems, *Phillips J. Res.* **39,** 1 (1984).
8. S. Wakao and Y. Yonemura, *J. Less-Common Met.* **131,** 311 (1981).
9. A. Zuttel, F. Meli and L. Schlapbach, *J. Alloy Comp.* **200,** 157 (1993).
10. C. S. Wang, X. H. Wang, Y. Q. Lei, C. P. Chen and Q. D. Wang, *Int. J. Hydrogen Energy* **21,** 471 (1996).
11. X. H. Wang, C. S. Wang, Y. Q. Lei, C. P. Chen and Q. D. Wang, *Int. J. Hydrogen Energy* **21,** 479 (1996).
12. Y. G. Yoon and S. I. Prun, *Electrochim. acta* **40,** 999 (1995).
13. C. S. Wang, Y. Q. Lei and Q. D. Wang, *J. Power Sources*, in press.
14. W. Schmickler and J. W. Shults, in *Modern Aspects of Electrochemistry*, ed. J. O. M. Bockris, B. E. Conway and R. E. White, Vol. 17. Plenum press, New York, 1986, Chap. 5, p. 257.
15. D. A. Porter, *Phase Transformation in Metal and Alloy*. Van Nostrand Reinhold, New York, 1981, p. 283.
16. J. Balei, *Int. J. Hydrogen Energy* **10,** 365 (1985).
17. C. S. Wang, X. H. Wang, Y. Q. Lei, C. P. Chen and Q. D. Wang, *Int. J. Hydrogen Energy* **22,** 1117 (1997).
18. P. H. L. Notten and P. Hokkeling, *J. Electrochem. Soc.* **138,** 1877 (1991).
19. G. Zhang, B. N. Popov and R. E. White, *J. Eletrochem. Soc.* **142,** 2695 (1995).
20. J. H. Jurg, K. Y. Lee and J. Y. Lee, *J. Alloys Comp.* **226,** 166 (1995).
21. R. Burch and N. B. Mason, *J. Chem. Soc. Faraday Trans.* **1,** 561 (1979).
22. P. H. L. Notten, R. E. F. Einerhend and J. L. C. Daams, *J. Alloys Comp.* **210,** 221 (1994).
23. C. Iwakura, M. Matsuoka and T. Kohno, *J. Electrochem. Soc.* **141,** 2306 (1994).